BUHEP–95–2

Top Quarks and Flavor Physics

Kenneth Lane†

Department of Physics, Boston University
590 Commonwealth Avenue, Boston, MA 02215

Abstract

Because of the top quark's very large mass, about 175 GeV, it now provides the best window into flavor physics. Thus, pair–production of top quarks at the Tevatron Collider is the best probe of this physics until the Large Hadron Collider turns on in the next century. I discuss aspects of the mass and angular distributions that can be measured in $t\bar{t}$ production with the coming large data samples from the Tevatron and even larger ones from the LHC.

1/95

† lane@buphyc.bu.edu

1. Introduction

The CDF collaboration has reported evidence for top–quark production at the Tevatron Collider [1]. According to these papers, the top mass is $m_t = 174 \pm 10\,^{+13}_{-12}\,\mathrm{GeV}$. The CDF data are based on an integrated luminosity of $19.3\,\mathrm{pb}^{-1}$. Taking into account detector efficiencies and acceptances, CDF reports the production cross section $\sigma(p\overline{p} \to t\bar{t}) = 13.9\,^{+6.1}_{-4.8}\,\mathrm{pb}$ at $\sqrt{s} = 1800\,\mathrm{GeV}$. The predicted QCD cross section for $m_t = 174\,\mathrm{GeV}$, including next–to–leading–log corrections [2], and soft–gluon resummation [3], is $\sigma(t\bar{t}) = 5.10^{+0.73}_{-0.43}\,\mathrm{pb}$. This is 2.8 times smaller than the central value of the measured cross section. The uncertainty in α_S increases the theoretical error in $\sigma(t\bar{t})$ to at most 30% [4].

Very recently, the DØ Collaboration has also reported evidence for top–quark production [5]. A direct measurement of the top–quark mass and cross section was not made by DØ in this report. However, assuming that the excess of signal events over expected background is due to $t\bar{t}$ production and that $m_t = 180\,\mathrm{GeV}$, DØ deduces the cross section $\sigma(t\bar{t}) = 8.2 \pm 5.1\,\mathrm{pb}$. This is consistent with the standard model and with CDF.

The experimental errors on the CDF and DØ measurements are large. Assuming the top mass is close to 175 GeV, the CDF cross section could be due to an up–fluctuation or to underestimated efficiencies (although the latter seems unlikely; see [1]). But, if it is confirmed by both experiments in their current higher–luminosity runs, the large $t\bar{t}$ rate heralds the long–awaited collapse of the standard model. Even if the standard model result is found in the new data, however, it is clear that the top quark provides a wide–open window into the world of flavor physics. It is the heaviest elementary particle we know and, more to the point, the heaviest elementary fermion by a factor of 40—as massive as tungsten. As a first example of flavor physics, we note that if the Higgs boson of the minimal one–doublet model exists, its coupling to the top quark, renormalized at $m_t = 174\,\mathrm{GeV}$, is large: $\Gamma_t = 2^{3/4}\,G_F^{1/2}\,m_t = 1.00$. If there are charged scalars, members of Higgs–boson multiplets or technipions, they are expected to couple to top quarks with $\mathcal{O}(1)$ strength and to decay as $H^+ \to t\bar{b}$. Recently, several papers have discussed aspects of flavor physics that are more or less intimately connected to the large top mass and that lead to enhanced rates of the $t\bar{t}$ signals studied by the Tevatron experiments [6], [7], [8].

In this paper, we discuss two distributions that may be used to distinguish alternative models of $t\bar{t}$ production—including standard QCD [9]. These are the invariant mass distribution, $d\sigma/d\mathcal{M}_{t\bar{t}}$, and the center–of–mass (c.m.) angular distribution of the top quark,

$d\sigma/d\cos\theta$. The magnitude and shape of the invariant mass distribution (Section 2) can reveal whether $t\bar{t}$ production is standard or not, and whether resonances decaying to $t\bar{t}$ exist. We point out that, for standard QCD production, the mean and root–mean–square invariant masses are linear functions of the top–quark mass over the entire interesting range of m_t. Thus, the $\mathcal{M}_{t\bar{t}}$ distribution can provide an *independent* determination of the top quark's mass. We apply this to the CDF data [1] and find quite good consistency with the directly measured mass. This analysis is made at the most elementary theoretical level. It needs to be carefully redone by the experimental collaborations themselves.

In Section 3, we apply the $\mathcal{M}_{t\bar{t}}$ analysis to examples of the three nonstandard mechanisms of $t\bar{t}$ production described in Refs. [6], [7] and [8]. The first involves resonant production of a 400–600 GeV color–octet vector meson ("coloron"), V_8, which is associated with electroweak symmetry breaking via top–condensation [10] and which interferes with QCD production via the process $q\overline{q} \to V_8 \to t\bar{t}$. The second example invokes a color–octet pseudoscalar, η_T [11]. In multiscale models of walking technicolor [12], [13], the η_T is produced strongly in gluon–gluon fusion and decays mainly to $t\bar{t}$. The third model has additional production of the classic $t\bar{t}$ signals [1]. This occurs through pair–production of an electroweak–*isoscalar*, color–triplet quark, t_s, which is approximately degenerate with the top quark and which, through mass–mixing, decays as $t_s \to W^+ b$. The agreement found in Section 2 between CDF's directly measured top–mass and that extracted from the $\mathcal{M}_{t\bar{t}}$ moments does not yet rule out these new mechanisms of top–quark production. The $\mathcal{M}_{t\bar{t}}$ distributions from the current Tevatron run may do so. (Of course, finding the standard model cross section will also be powerful evidence against alternative production mechanisms.)

The angular distribution of top quarks (Section 4) also reflects the underlying production mechanism. Even though most of $t\bar{t}$ production is near threshold, the expectation that it is mainly s–wave can be overturned if there are large parity–violating components in the $q\overline{q} \to t\bar{t}$ process. We shall compare the angular distributions for standard and nonstandard $t\bar{t}$ production at the Tevatron and at the CERN Large Hadron Collider. We shall see that, because of the much larger $\tau = \hat{s}/s$ in top–pair production at the Tevatron, experiments there have an advantage over those at the LHC.[1] These angular tests require much larger

[1] In this paper I do not discuss high–energy e^+e^- colliders such as the 500 GeV (or so) NLC. Our focus is on distinguishing alternate mechanisms of $t\bar{t}$ production. Lepton machines cast no light on such strongly–coupled flavor physics aspects of $t\bar{t}$ production as the V_8 and η_T. The higher rates possible at hadron machines also make them ideal for searches for new particles such as charged scalars in the decays of top quarks.

data sets than will be available in the next year or two. To realize the full potential of this handle on flavor physics, it is essential that the Tevatron experiments be able to collect samples as large as 1–10 fb^{-1}.

2. Invariant Mass Distributions In QCD

Strictly speaking, the $t\bar{t}$ invariant mass $\mathcal{M}_{t\bar{t}}$ is not well–defined in QCD because of the emission of soft and collinear gluons from the t and $\bar{t}$ quarks. Nevertheless, the theoretical invariant mass is numerically not very different from a definition of $\mathcal{M}_{t\bar{t}}$ that allows for this gluon radiation. Furthermore, because the p_T of the $t\bar{t}$ c.m. system typically is small compared to m_t, it will be a good approximation for us to use the lowest–order QCD cross section $d\sigma/d\mathcal{M}_{t\bar{t}}$ to discuss the moments of the invariant mass distribution. This distribution is shown in Fig. 1 for the Tevatron Collider and for top–quark masses in the interesting range 100–220 GeV.[2] The mass distributions are seen to be sharply peaked at $\mathcal{M}_{\rm max} \simeq 2.1 m_t + 10\,{\rm GeV}$. Consequently, low moments of the mass distribution, the mean and RMS, are nearly linear functions of the top–quark mass (also see Ref. [15]). For $100 \lesssim m_t \lesssim 200\,{\rm GeV}$, the first two moments are well–fit by the formulae

$$\begin{aligned} \langle \mathcal{M}_{t\bar{t}} \rangle &= 50.0\,{\rm GeV} + 2.24\,m_t \\ \langle \mathcal{M}^2_{t\bar{t}} \rangle^{1/2} &= 58.4\,{\rm GeV} + 2.23\,m_t\,. \end{aligned} \tag{2.1}$$

In the range $m_t \simeq$ 140–200 GeV, the dispersion in $\mathcal{M}_{t\bar{t}}$ expected for standard QCD production is $\Delta\mathcal{M}_{t\bar{t}} =$ 70–80 GeV.[3]

---

[2] These plots and all other calculations in this paper were carried out using lowest–order QCD subprocess cross sections and the EHLQ Set 1 parton distribution functions [14]. To account for QCD radiative corrections, our $t\bar{t}$ cross sections have been multiplied by 1.62. This makes our QCD rates and the central values quoted in Ref. [3] agree to within one per cent over the entire interesting range of top masses. Our numerical results for the linear dependence of $\langle \mathcal{M}_{t\bar{t}} \rangle$ and $\langle \mathcal{M}^2_{t\bar{t}} \rangle^{1/2}$ on m_t are accurate so long as the higher–order corrections are well–represented by a simple multiplicative factor.

[3] If there are experimental difficulties in measuring $\mathcal{M}_{t\bar{t}}$ that do not also affect the measurement of m_t, one could instead use the mean value of the summed scalar–E_T to extract the top–quark mass. Indeed, in Ref. [15], it was shown that a quantity as indirect as the invariant mass $\mathcal{M}_{e\mu}$ of the isolated electron plus muon measured in $t\bar{t} \to e^{\pm} + \mu^{\mp} +$ jets is also a linear function of m_t and may be used to determine it.

In Ref. [1], the top quark mass was determined from a sample of seven $W \to \ell\nu$ + 4 jets events by making an overall constrained best fit to the hypothesis $p\overline{p} \to t\overline{t} + X$, followed by the standard top decays $t \to W^+ b$ with one W decaying leptonically and the other hadronically. At least one of the b–jets was tagged. The CDF paper provides the momentum 4–vectors of all particles in the event before and after the constrained fit. From these, the central values of kinematic characteristics of the seven events may be determined. Table 1 lists the best–fit top–quark masses determined by CDF together with the invariant mass of the events before and after the constrained fit.[4] We used these $\mathcal{M}_{t\bar{t}}$ to compute the mean and RMS. Both sets of 4–momenta gave essentially identical results. Using 4–momenta from the constrained fit, we found:

$$\begin{aligned} \langle \mathcal{M}_{t\bar{t}} \rangle &= 439 \pm 11\,\mathrm{GeV} \quad \Longrightarrow \quad m_t = 173 \pm 5\,\mathrm{GeV} \\ \langle \mathcal{M}^2_{t\bar{t}} \rangle^{1/2} &= 443 \pm 11\,\mathrm{GeV} \quad \Longrightarrow \quad m_t = 172 \pm 5\,\mathrm{GeV} \\ \Delta\mathcal{M}_{t\bar{t}} &= 59.5\,\mathrm{GeV}\,. \end{aligned} \tag{2.2}$$

The errors in Eq. (2.2) were estimated by the "jacknife" method of computing the moments while omitting one of the seven events. They give some sense of the theoretical error in determining the mean and RMS invariant masses from the limited CDF sample. They are *not* to be interpreted as the true experimental errors; the CDF group must provide those. However, we expect that the process of averaging the invariant mass will give moderately small experimental errors.

These results give some confidence that CDF's measured central value of the top–quark mass, 174 GeV, is accurate. For example, if $m_t = 160\,\mathrm{GeV}$ (for which Ref. [3] predicts $\sigma(t\bar{t}) = 8.2^{+1.3}_{-0.8}\,\mathrm{pb}$), we would expect $\langle \mathcal{M}_{t\bar{t}} \rangle = 409\,\mathrm{GeV}$ and $\langle \mathcal{M}^2_{t\bar{t}} \rangle^{1/2} = 415\,\mathrm{GeV}$, well below the values determined above. Thus, if something is going to change in the CDF results from the current run, we expect it will be the cross section—which needs to become two to three times smaller to agree with the standard model.

[4] Particle 4–vectors before the constrained fit do have various corrections—e.g., for the jet energy scale—made to them [1]. Only $\not\!\!E_T$ is provided for the neutrino(s) in the before–fit 4–vectors. The biggest change in the before and after momenta occurs in $\not\!\!E_T$. We used the $W \to \ell\nu$ 4–momenta determined from the constrained fit in both cases.

3. Nonstandard Mass Distributions

In this section we examine three nonstandard proposals [6], [7], [8] for $t\bar{t}$ production and the large cross section reported by CDF [1]. We shall find that they are not yet disfavored by the good agreement between the central values of the measured top mass and the top masses deduced in Eq. (2.2). We begin by quoting the differential cross sections for $q\overline{q} \to t\bar{t}$ and $gg \to t\bar{t}$ in lowest–order QCD:

$$\frac{d\hat{\sigma}(q\overline{q} \to t\bar{t})}{dz} = \frac{\pi\alpha_s^2\beta}{9\hat{s}}\left(2 - \beta^2 + \beta^2 z^2\right),$$

$$\frac{d\hat{\sigma}(gg \to t\bar{t})}{dz} = \frac{\pi\alpha_s^2\beta}{6\hat{s}}\left\{\frac{1+\beta^2 z^2}{1-\beta^2 z^2} - \frac{(1-\beta^2)^2\,(1+\beta^2 z^2)}{(1-\beta^2 z^2)^2} - \tfrac{9}{16}(1+\beta^2 z^2) + \frac{1-\beta^2}{1-\beta^2 z^2}\,(1 - \tfrac{1}{8}\beta^2 + \tfrac{3}{8}\beta^2 z^2)\right\}, \tag{3.1}$$

where $z = \cos\theta$, θ is the c.m. scattering variable and $\beta = \sqrt{1 - 4m_t^2/\hat{s}}$. For $\hat{s} \gg 4m_t^2$, these cross sections—especially the gluon fusion one—are forward–backward peaked. But, at the modest $\hat{s}$ at which QCD $t\bar{t}$ production is large, the cross sections are fairly isotropic.

For the "coloron" bosons of Ref. [6], we adopted a version of the model in which the gauge symmetry $SU(3)_1 \otimes SU(3)_2$ breaks down to color $SU(3)$, yielding eight massless gluons and equal-mass V_8's. To study parity violation in the angular distributions in $t\bar{t}$ production (see Section 4), we made the theoretically inane assumption that the V_8 couples only to left–handed quarks with the amplitude

$$A(V_8^a(p,\lambda) \to q(p_1)\,\overline{q}(p_2)) = g_s\,\xi_q\,\epsilon^\mu(p,\lambda)\,\overline{u}_q(p_1)\,\frac{\lambda_a}{2}\,\gamma_\mu\,\left(\frac{1-\gamma_5}{2}\right)\,v_q(p_2)\,. \tag{3.2}$$

Here, g_s is the QCD coupling and, following Ref. [6], we took $\xi_t = \xi_b = \pm 1/\xi_q$ ($q = u, d, c, s$). For this chiral coupling, the $q\overline{q} \to t\bar{t}$ angular distribution in Eq. (3.1) is modified by the addition of

$$\frac{d\hat{\sigma}(q\overline{q} \to V_8 \to t\bar{t})}{dz} = \frac{\pi\alpha_s^2\beta}{36\hat{s}}\,(1+\beta z)^2\,\left\{\left|1 + \xi_q\,\xi_t\,\frac{\hat{s}}{\hat{s} - M_{V_8}^2 + i\sqrt{\hat{s}}\,\Gamma(V_8)}\right|^2 - 1\right\}, \tag{3.3}$$

where, ignoring the mass of all quarks except the top's, the V_8 width is

$$\Gamma(V_8) = \frac{\alpha_s M_{V_8}}{12}\left\{4\xi_q^2 + \xi_t^2\left(1 + \beta_t(1 - m_t^2/M_{V_8}^2)\right)\right\}, \tag{3.4}$$

where $\beta_t = \sqrt{1 - 4m_t^2/M_{V_8}^2}$.

The $\mathcal{M}_{t\bar{t}}$ distribution in the coloron model for $M_{V_8} = 450\,\mathrm{GeV}$ is shown in Fig. 3 for $\xi_t = \xi_b = -1/\xi_q = \sqrt{40/3}$ (see [6]) and in Fig. 4 for $\xi_t = \xi_b = 1/\xi_q = \sqrt{40/3}$. The effect of interference with the QCD amplitude is obvious as is the tendency for the $\mathcal{M}_{t\bar{t}}$ distribution to be enhanced at lower (higher) masses for $\xi_t = -1/\xi_q$ $(+1/\xi_q)$. The theoretical width of the V_8 in this example is $\Gamma(V_8) \cong \Gamma(V_8 \to b\bar{b}) + \Gamma(V_8 \to t\bar{t}) = 40\,\mathrm{GeV}$. Figures 5 and 6 show the mass distibutions for $M_{V_8} = 475\,\mathrm{GeV}$ and $\xi_t = \mp\xi_b = \sqrt{40/3}$. Here, $\Gamma(V_8) \cong 85\,\mathrm{GeV}$ and the mass distribution is significantly broader than in the case of $M_{V_8} = 450\,\mathrm{GeV}$. The characteristics of these mass distributions will be discussed below together with those of the other nonstandard production models we are considering.[5]

Many technicolor models contain a color–octet pseudoscalar boson, η_T. So long as the η_T may be treated as a pseudo–Goldstone boson, its decay rates to gluons can be computed from the triangle anomaly [11]. We introduce a dimensionless factor C_q in the Yukawa coupling of η_T to $q\overline{q}$ [7]. While it is determined by the details of the underlying extended technicolor model, we expect $C_q = \mathcal{O}(1)$. Then, the η_T's main decay modes are to two gluons and $t\bar{t}$ and they are given by

$$\begin{aligned} \Gamma(\eta_T \to gg) &= \frac{5\alpha_s^2\, N_{TC}^2\, M_{\eta_T}^3}{384\,\pi^3\, F_Q^2}\,, \\ \Gamma(\eta_T \to t\bar{t}) &= \frac{C_t^2\, m_t^2\, M_{\eta_T}\, \beta_t}{16\pi F_Q^2}\,. \end{aligned} \tag{3.5}$$

The gluon fusion cross section for $t\bar{t}$ production is modified by the addition of

$$\begin{aligned} \frac{d\hat{\sigma}(gg \to \eta_T \to t\bar{t})}{dz} =& \frac{\pi}{4}\, \frac{\Gamma(\eta_T \to gg)\,\Gamma(\eta_T \to t\bar{t})}{(\hat{s} - M_{\eta_T}^2)^2 + \hat{s}\,\Gamma^2(\eta_T)} \\ &+ \frac{5\sqrt{2}\,\alpha_s^2\, N_{TC}\, C_t\, m_t^2\, \beta}{768\pi F_Q^2}\, \frac{\hat{s} - M_{\eta_T}^2}{(\hat{s} - M_{\eta_T}^2)^2 + \hat{s}\,\Gamma^2(\eta_T)}\, \frac{1 - 2\beta^2 z^2}{1 - \beta^2 z^2}\,. \end{aligned} \tag{3.6}$$

In these expressions, it is assumed that the η_T is composed from a single doublet of techniquarks $Q = (U, D)$ in the $\mathbf{N_{TC}}$ representation of $SU(N_{TC})$; F_Q is the decay constant of technipions in the $\overline{Q}Q$ sector. The first term on the right is isotropic; the second

[5] Note that this V_8 model predicts a strong resonance in $q\overline{q} \to b\bar{b}$, providing another good way to to test it.

(interference) term is never very important, but we include it for completeness. In the narrow resonance approximation, the contribution of the η_T to the $pp^{\pm} \to t\bar{t}$ rate,

$$\sigma(pp^{\pm} \to \eta_T \to t\bar{t}) \simeq \frac{\pi^2}{2s} \frac{\Gamma(\eta_T \to gg)\,\Gamma(\eta_T \to t\bar{t})}{M_{\eta_T}\,\Gamma(\eta_T)} \times \int d\eta_B\, f_g^p\left(\frac{M_{\eta_T}}{\sqrt{s}} e^{\eta_B}\right) f_g^p\left(\frac{M_{\eta_T}}{\sqrt{s}} e^{-\eta_B}\right), \tag{3.7}$$

scales as N_{TC}^2/F_Q^2. Here, η_B is the boost rapidity of the $t\bar{t}$ c.m. frame and $f_g^p(x)$ is the gluon distribution function for the proton for mommentum fraction x and $Q^2 = M_{\eta_T}^2$.

As discussed in Ref. [7], the η_T of the standard one–family technicolor model [11] has $F_Q = 123\,\mathrm{GeV}$ and, for $N_{TC} \lesssim 8$, it cannot significantly increase the $t\bar{t}$ rate at the Tevatron. Thus, we were motivated to consider the η_T arising in multiscale models [12] of walking technicolor [13]. Multiscale models are characterized by a small η_T decay constant; for the calculations presented here, we chose $F_Q = 30\,\mathrm{GeV}$. The mass distribution for a model with $N_{TC} = 5$ and $C_t = -1/3$ is shown in Fig. 7 for $M_{\eta_T} = 450\,\mathrm{GeV}$. The width of the η_T in this case is $\Gamma(\eta_T) \cong \Gamma(\eta_T \to t\bar{t}) + \Gamma(\eta_T \to gg) = 21\,\mathrm{GeV} + 11\,\mathrm{GeV} = 32\,\mathrm{GeV}$. Figure 8 shows the cross section for $M_{\eta_T} = 475\,\mathrm{GeV}$; in this case, $\Gamma(\eta_T) \cong 37\,\mathrm{GeV}$. In both cases, the small decay constant results in a rate 2–3 times larger than QCD.

The third model of enhanced top–production we considered is one in which an electroweak–isoscalar, charge $\frac{2}{3}$ quark, t_s, is approximately degenerate with the top–quark and mixes with it so that both have the same Wb decay mode [8]. If $m_{t_s} = m_t = 174\,\mathrm{GeV}$ the expected rate for the top–quark signal is doubled to 10.2 pb. We illustrate the isoscalar quark model in Figs. 9 and 10 with two cases: $m_{t_s} = 160$ and $m_t = 175\,\mathrm{GeV}$; $m_{t_s} = 165$ and $m_t = 190\,\mathrm{GeV}$.

Before discussing features of these nonstandard $\mathcal{M}_{t\bar{t}}$ distributions, a comment on radiative corrections is in order. As noted above, we have multiplied all our lowest–order EHLQ1 cross sections by the factor 1.62. This is a composite of the radiative corrections *at the Tevatron* for the purely QCD processes $gg \to t\bar{t}$ and $q\overline{q} \to t\bar{t}$. For a 1.8 TeV $p\overline{p}$ collider, the $q\overline{q}$ process accounts for 90% of heavy $t\bar{t}$ production in the standard model.[6] On the other hand, the gluon fusion process receives the largest radiative correction [2], [3]. We do not know the radiative corrections appropriate to the resonant production processes $q\overline{q} \to V_8 \to t\bar{t}$ and $gg \to \eta_T \to t\bar{t}$, but it seems likely that our multiplication by 1.62

[6] This situation is reversed at the 15 TeV LHC pp collider, where $gg \to t\bar{t}$ is 90% of the QCD cross section.

overestimates the former and underestimates the latter process. Thus, the total Tevatron cross sections for these processes may be accurate to only about 30%.

The total $t\bar{t}$ cross sections at the Tevatron and the characteristics extracted from the $\mathcal{M}_{t\bar{t}}$ distributions are displayed in Table 2 for the CDF data (see Eq. (2.2)) and for the three nonstandard production models described above. We note the following features:

1.) The CDF data is narrower ($\Delta\mathcal{M}_{t\bar{t}} = 60\,\mathrm{GeV}$) than the QCD expectation (77 GeV). While this $\Delta\mathcal{M}_{t\bar{t}}$ is consistent with the resonant production models, the statistics are so low that we do not consider this significant. It is a feature worth watching for in future data samples.
2.) If $\xi_q\xi_t = -1$ in the coloron model (corresponding to the notation V_8^- in Table 2), the mass distribution is increased below the resonance and depressed above it; vice-versa for $\xi_q\xi_t = +1$ (V_8^+). We see that, for a given M_{V_8}, this results in an extracted value of m_t that is somewhat smaller than or *significantly* larger than the directly–measured one, depending on whether $\xi_q\xi_t = -1$ or $+1$.
3.) The η_T's we have considered are narrow enough to not interfere appreciably with the QCD gluon fusion process. Thus, the value of the extracted top mass depends mainly on M_{η_T}; it tends to be larger for a larger M_{η_T}, but then the η_T rate becomes smaller and the distortion of $\sigma(t\bar{t})$ less important. Resonance masses in the range 400–500 GeV return a top mass close to the directly–measured value.
4.) It is easy to double the QCD value of $\sigma(t\bar{t})$ in the isoscalar quark model: just choose $m_{t_s} = m_t$. But, as could be foreseen, it is difficult for the isoscalar quark model to give both a 13.9 pb cross section and an extracted mass close to the directly–measured one. To get a cross section ~ 3 times as large as QCD requires choosing one of the masses significantly lower than 174 GeV, leading to too small an extracted value. This model could be the easiest to eliminate with data from the current Tevatron run.

Finally, we remark that subsystem invariant masses may be as interesting as the total invariant mass. For example, in multiscale technicolor, it is possible that a color–octet technirho is produced and decays as $\rho_T \to W^{\mp}\pi_T^{\pm}$, with $\pi_T^+ \to t\bar{b} \to W^+b\bar{b}$, the *same* final state as in $t\bar{t}$ production [12]. Searches for processes such as these, using a constrained–fit procedure analogous to that employed by CDF for the $t\bar{t}$ hypothesis, should be carried out. All this will require a lot of data from the Tevatron, perhaps $1\,\mathrm{fb}^{-1}$ or more. At the expense of increasing backgrounds, larger data samples may be had by using appropriately selected events *without* a tagged b–jet. This was done in Ref. [1] and was found to give an excess of events with constrained–fit m_t above 160 GeV.

4. Angular Distributions

The $t\bar{t}$ angular distribution of top quarks also provides information about their production mechanism. The distribution expected in lowest–order QCD was given in Eq. (3.1). As we noted, the $gg \to t\bar{t}$ process—10% of the QCD rate at the Tevatron and 90% of it at the LHC—is strongly forward–backward peaked at $\hat{s} \gg 4\ m_t^2$, but fairly isotropic near threshold where most $t\bar{t}$ production occurs. Resonances such as the top–color V_8 and the technicolor η_T may change the proportion of gg and $q\bar{q}$–induced $t\bar{t}$ production and the top angular distribution at these colliders.

By Bose symmetry, the angular distribution in $gg \to t\bar{t}$ processes is forward–backward symmetric. Although this is also true in lowest–order QCD for $q\bar{q} \to t\bar{t}$, there is no reason it need be so for nonstandard production mechanisms. To illustrate the ability of hadron collider experiments to distinguish different angular distributions, we assume that the coloron V_8 couples only to left–handed quarks, implying the angular distribution $(1 + \beta \cos\theta)^2$.

The Tevatron has a distinct advantage in the study of top angular distributions. To determine θ in $q\bar{q} \to t\bar{t}$ processes, we need to know the direction of the incoming light quark as well as that of the outgoing top quark.[7] In $p\bar{p} \to t\bar{t}$ at $\sqrt{s} = 1800\,\mathrm{GeV}$, the q–direction is the same as that of the proton practically all the time. Thus, if we denote by θ^* the angle between the proton direction and the top–quark direction in the subprocess c.m., this angle is almost always the same as θ. As we shall see, the Tevatron's analyzing power would be significantly improved if the luminosity of the Tevatron were increased to $10^{33}\,\mathrm{cm}^{-2}\,\mathrm{s}^{-1}$ or more and its detectors upgraded to handle this luminosity.

In pp collisions, the direction of the incoming quark can be inferred with confidence only for events with high boost rapidity, η_B, or large fractional subprocess energy, $\tau = \hat{s}/s$. (For pp collisions, θ^* will be defined as the angle between the direction of the boost and that of the top quark in the subprocess c.m.) For large τ, the quark direction tends to be the same as the boost of the c.m., even if η_B is small [15]. However, τ is small for $q\bar{q} \to t\bar{t}$ at the LHC, making it hard to distinguish θ from $\pi - \theta$. To make matters worse, $t\bar{t}$ production is dominated by gluon fusion, obscuring any interesting $\cos\theta$ dependence. Thus, angular information on top production is doubly difficult to come by at the LHC.

[7] The distinction between t and $\bar{t}$ is based on the sign of the charged lepton in W–decay.

The $\cos\theta^*$ distributions we present below are integrals over $t\bar{t}$ invariant mass of $d\sigma(pp^{\mp} \to t\bar{t})/d\mathcal{M}_{t\bar{t}}\, d\cos\theta^*$. The integration region is centered on the peak of the invariant mass distribution and is approximately the width of the resonance. For the η_T, we used $M_{\eta_T} = 450\,\mathrm{GeV}$, $N_{TC} = 5$, $F_Q = 30\,\mathrm{GeV}$ and $C_t = -1/3$. Its width is 32 GeV. For the V_8, we took $M_{V_8} = 475\,\mathrm{GeV}$ and $\xi_t = \mp 1/\xi_q = \sqrt{40/3}$. The V_8 width is 85 GeV.

The $\cos\theta^*$ distributions, defined as described above for $p\overline{p}$ (Tevatron) and pp (LHC) collisions, are shown for the η_T and V_8 models in Figs. 11–14. Global features of these distributions are summarized in Table 3. The top quarks were required to have pseudorapidity $|\eta| < 2$, which we estimate to correspond to the average acceptance of the CDF and DØ detectors for leptons and jets from top decay.[8] We discuss them in turn:

Figure 11 shows the $q\overline{q} \to t\bar{t}$, $gg \to t\bar{t}$ and $gg \to \eta_T \to t\bar{t}$ components of the top–production $\cos\theta^*$ distribution expected at the Tevatron. The $\mathcal{M}_{t\bar{t}}$ integration region is 430 to 470 GeV. The QCD contribution is flat, the forward–backward peaking diminished by the proximity of threshold. The η_T contribution is also flat, of course, and makes up about 85% of the total cross section. The falloff above $|\cos\theta^*| = 0.90$ is due to the rapidity cut, $|\eta_{t,\bar{t}}| < 2.0$. (We computed the $\cos\theta^*$ distribution of the seven $t\bar{t}$ candidate events reported by CDF [1]. The results, along with the top quark's c.m. velocity β, are listed in Table 1. They form a perfectly flat distribution.) Table 3 lists the total $t\bar{t}$ cross section as well as the cross sections σ_F for $\cos\theta^* > 0$ and σ_B for $\cos\theta^* < 0$. The forward-backward asymmetry is calculated as

$$A_{FB} = \frac{N_F - N_B}{N_F + N_B} = \frac{\sigma_F - \sigma_B}{\sigma_F + \sigma_B}\,. \tag{4.1}$$

The statistical error on A_{FB} is

$$(\Delta A_{FB})_{\mathrm{stat}} = 2\sqrt{\frac{N_F N_B}{(N_F + N_B)^3}} = 2\sqrt{\frac{\sigma_F \sigma_B}{(\sigma_F + \sigma_B)^3\, \epsilon_{t\bar{t}} \int \mathcal{L}dt}}\,, \tag{4.2}$$

where $\epsilon_{t\bar{t}}$ is the overall efficiency, including branching ratios, for identifying and reconstructing $t\bar{t}$ events. For the CDF experiment at the Tevatron, we can infer from Ref. [1] that $\epsilon_{t\bar{t}}(\mathrm{CDF}) \simeq$ 5–10 events/$(19\,\mathrm{pb}^{-1} \times 14\,\mathrm{pb})$ = 2–4%. We use $\epsilon_{t\bar{t}}(\mathrm{TEV}) = 3\%$. It is difficult to say what value of the efficiency is appropriate for LHC experiments; detailed

[8] Our results do not change significantly if we require $|\eta| < 1.5$ for the Tevatron detectors and allow $|\eta| < 2.5$ for the LHC detectors.

simulations are needed (see e.g., Ref. [15]). We shall assume $\epsilon_{t\bar{t}}(\mathrm{LHC}) = 5\%$, although it turns out not to matter in the examples we consider.

The components of the $\cos\theta^*$ distribution expected at the LHC are shown in Fig. 12. Because of the small τ values involved, the roles of gluon fusion and $q\overline{q}$ annihilation are reversed, with gluon fusion making up about 90% of the QCD rate. The enormous $\eta_T \to t\bar{t}$ rate is due to the very large gg luminosity at small τ [14]. The slight central bowing of the $\cos\theta^*$ distribution is due to the top–rapidity cut. At the LHC energy, such large boost rapidities occur that events at large c.m. rapidity and $\cos\theta^*$ are depleted.

Figure 13 shows the components of the $\cos\theta^*$ distribution at the Tevatron for the 475 GeV V_8 coupling to left–handed quarks with relative strengths $\xi_t = -1/\xi_q = \sqrt{40/3}$. The $\mathcal{M}_{t\bar{t}}$ integration region is 400–500 GeV. The effect of the chiral coupling is evident, though somewhat diminished by the $\eta_{t,\bar{t}}$ cut. The forward–backward asymmetry of 0.35 could be measured at the 5σ (statistical) level with an integrated luminosity of $1\,\mathrm{fb}^{-1}$. For this luminosity, the statistical errors on $d\sigma/d\cos\theta^*$ in six bins 0.30 units wide would range from 20% down to 10%. This is one example of how useful it would be to upgrade the Tevatron luminosity to $10^{33}\,\mathrm{cm}^{-2}\,\mathrm{s}^{-1}$.

The $\cos\theta^*$ distributions expected at the LHC for this V_8 are shown in Fig. 14. In this example, the contribution of the V_8 is about 20% of the total and it is polluted by the $q \leftrightarrow \overline{q}$ ambiguity, so that the rise in the cross section with $\cos\theta^*$ is invisible. The asymmetry is only 2%. This illustrates the dominance of gg processes and the uncertainty in determining the quark direction at small τ in a high–energy pp collider. Essentially similar results were obtained for the $\xi_t = 1/\xi_q$ case (see Table 3). We found that there is nothing to be gained at the LHC by a looser η_t cut, or by limiting the $\mathcal{M}_{t\bar{t}}$ integration region to a narrow band about M_{V_8}, or by selecting events produced at large boost rapidity.

5. Summary

Top quarks, of all known elementary particles, are most intimately connected to the physics of flavor and may provide keys to unlock its mysteries. Thus, top–quark production at the Tevatron provides our most incisive probe into flavor physics until the LHC turns on in the next century. The invariant mass distributions that can be formed in top–quark production appear to be the best means for distinguishing between standard and nonstandard mechanisms.

The mean and RMS of the total invariant mass, $\mathcal{M}_{t\bar{t}}$, provide an independent measure of m_t which should agree with the directly–measured mass *if* production is governed by standard QCD. In QCD, the variance $\Delta\mathcal{M}_{t\bar{t}}$ is expected to be about 75 GeV. The total invariant mass can reveal the presence of $t\bar{t}$ resonances such as the top–color vectors V_8 [6],[10] and the technihadron η_T [7],[11]. Such resonances may easily double the $t\bar{t}$ rate. It is worth noting that, since the fraction of gluon–initiated processes rises fairly rapidly as the machine energy, an upgrade of the Tevatron to $\sqrt{s} = 2\,\mathrm{TeV}$ will lead to quite different changes in the $V_8 \to t\bar{t}$ and $\eta_T \to t\bar{t}$ rates.[9] We find an increase of about 50% for $q\overline{q} \to V_8$, but almost 100% for $gg \to \eta_T$. Subsystem invariant masses can be examined for alternative explanations of the top–production data and for unconventional top decays. In this regard, we emphasize that it may be dangerous to use the standard QCD $t\bar{t}$ production model to select top–candidate events. For example, a resonance in $t\bar{t}$ production may distort the summed scalar–E_T and sphericity or aplanarity distributions of candidate events from their QCD expectation.

The angular dependence of top–production may also provide valuable information on the top–production mechanism. Although it is generally expected that, for production near threshold, the angular distribution will be isotropic, we have seen that chiral couplings can be detected if they are present and comparable to the QCD amplitudes. The dominance of $q\overline{q}$ annihilation in top–quark production processes at the Tevatron collider gives it an advantage over the LHC for studying angular distributions. Two distributions as different as those arising from the scalar–coupled η_T and the chiral–coupled V_8 may be distinguished with a data sample of $1\,\mathrm{fb}^{-1}$. However, it is clear that the resolving power of these distributions would benefit greatly from a significant upgrade of the collider and its detectors so that samples of $\mathcal{O}(10\,\mathrm{fb}^{-1})$ can be collected.

In conclusion, we emphasize that the studies done here have all been at the most naive parton level. We hope they will inspire the CDF and D$\emptyset$ collaborations to undertake more realistic, detector–specific simulations in the not–too–distant future.

I am indebted to Alessandra Caner, Sekhar Chivukula, Estia Eichten, John Huth, Chris Quigg, Elizabeth Simmons, John Terning and Avi Yagil for helpful conversations. This research was supported in part by the Department of Energy under Grant No. DE–FG02–91ER40676.

[9] I thank S. Parke for emphasizing this point to me.

References

[1] F. Abe, et al., The CDF Collaboration, Phys. Rev. Lett. **73**, 225 (1994); Phys. Rev. **D50**, 2966 (1994).

[2] P. Nason, S. Dawson, and R. K. Ellis, Nucl. Phys. **B303** (1988) 607; W. Beenakker, H. Kuijf, W. L. van Neerven and J. Smith, Phys. Rev. **D40** (1989) 54.

[3] E. Laenen, J. Smith and W. L. Van Neerven, Nucl. Phys. **B369** (1992) 543; *ibid*, FERMILAB–Pub–93/270–T.

[4] K. Ellis, "Top–Quark Production Rates in the Standard Model", invited talk at the 27th International Conference on High Energy Physics, Glasgow, 20–27th July 1994.

[5] S. Abachi, et al., The DØ Collaboration, "Search for High Mass Top Quark Production in $p\overline{p}$ Collisions at $\sqrt{s} = 1.8\,\mathrm{TeV}$", hep-ex–9411001, submitted to Physical Review Letters, November 9, 1994.

[6] C. Hill and S. Parke, Phys. Rev. **D49**, 4454 (1994)

[7] E. Eichten and K. Lane, Phys. Lett. **B327**, 129 (1994).

[8] V. Barger and R.J.N. Phillips, U. Wisconsin Preprint, MAD/PH/830 (May 1994).

[9] An abridged version of this work was given in K. Lane, "Top–Quark Production and Flavor Physics—The Talk", to appear in the Proceedings of the 27th International Conference on High Energy Physics, Glasgow, 20–27th July 1994; Boston University Preprint BUHEP–94–25 (1994).

[10] C. T. Hill, Phys. Lett. **266B**, 419 (1991);
S. P. Martin, Phys. Rev. **D45**, 4283 (1992); *ibid***D46**, 2197 (1992).

[11] E. Farhi and L. Susskind Phys. Rev. **D20** (1979) 3404;
S. Dimopoulos, Nucl. Phys. **B168** (1980) 69 ;
T. Appelquist and G. Triantaphyllou, Phys. Rev. Lett. **69**,2750 (1992) ;
T. Appelquist and J. Terning, Phys. Rev. **D50**, 2116 (1994).

[12] K. Lane and E. Eichten, Phys. Lett. **222B** (1989) 274 ;
K. Lane and M V. Ramana, Phys. Rev. **D44** (1991) 2678.

[13] B. Holdom, Phys. Rev. **D24** (1981) 1441; Phys. Lett. **150B** (1985) 301 ;
T. Appelquist, D. Karabali and L. C. R. Wijewardhana, Phys. Rev. Lett. **57** (1986) 957 ; T. Appelquist and L. C. R. Wijewardhana, Phys. Rev. **D36** (1987) 568 ;
K. Yamawaki, M. Bando and K. Matumoto, Phys. Rev. Lett. **56**, (1986) 1335 ;
T. Akiba and T. Yanagida, Phys. Lett. **169B** (1986) 432.

[14] E. Eichten, I. Hinchliffe, K. Lane and C. Quigg, Rev. Mod. Phys. **56**, 579 (1984).

[15] *GEM Technical Design Report*, Chapter 2; GEM TN–93–262, SSCL–SR–1219; Submitted by the GEM Collaboration to the Superconducting Super Collider Laboratory (April 30, 1993);
K. Lane, F. Paige, T. Skwarnicki and J. Womersley, *Simulations of Supercollider Physics*, hep-ph–9412280, submitted to Physics Reports.

Run—Event	m_t	$\mathcal{M}_{t\bar{t}}$(before fit)	$\mathcal{M}_{t\bar{t}}$(after fit)	β(after fit)	$\cos\theta^*$
40758–44414	172 ± 11	523	526	0.757	0.404
43096–47223	166 ± 11	533	511	0.760	0.820
43351–266423	158 ± 18	440	460	0.727	0.512
45610–139604	180 ± 9	338	366	0.180	−0.0011
45705–54765	188 ± 19	440	431	0.489	−0.348
45879–123158	169 ± 10	411	412	0.572	−0.767
45880–31838	132 ± 8	384	365	0.691	−0.682

Table 1. Best fit top–quark masses and kinematic characteristics of the CDF experiment's $t\bar{t}$ candidate events (from Ref. [1]). Masses are in GeV. Transverse motion of the subprocess c.m. was neglected in determining the top–quark velocity β and scattering angle θ^*.

Model	$\sigma(t\bar{t})$	$\langle\mathcal{M}_{t\bar{t}}\rangle$	$m_t\,(\langle\mathcal{M}_{t\bar{t}}\rangle)$	$\langle\mathcal{M}^2_{t\bar{t}}\rangle^{1/2}$	$m_t\,(\langle\mathcal{M}^2_{t\bar{t}}\rangle^{1/2})$	$\Delta\mathcal{M}_{t\bar{t}}$
LO–QCD (EHLQ1)	5.13	440	174	447	174	77
CDF data	$13.9^{+6.1}_{-4.8}$	439	173	443	172	60
$M_{V_8^-} = 450$	13.3	431	170	433	168	46
$M_{V_8^+} = 450$	11.0	465	185	469	184	58
$M_{V_8^-} = 475$	14.9	440	174	444	173	53
$M_{V_8^+} = 475$	10.8	482	193	487	192	67
$M_{\eta_T} = 450$	13.5	432	171	435	169	52
$M_{\eta_T} = 475$	11.4	442	175	446	174	55
$t_s(160)$ $t(175)$	13.2	421	166	428	166	77
$t_s(165)$ $t(190)$	10.0	437	173	444	173	77

Table 2. $p\bar{p} \to t\bar{t}$ cross sections (in pb) at $\sqrt{s} = 1800\,\mathrm{GeV}$ and their kinematic characteristics for lowest–order QCD, CDF data [1], and the three nonstandard production models with parameters described in the text. Cross sections have been multiplied by 1.62.

Model	$\mathcal{M}_{t\bar{t}}$ range	Collider	$\sigma(t\bar{t})$	σ_F	σ_B	A_{FB}
η_T	$430-470$	TEV	4.82	2.41	2.41	0
η_T	$430-470$	LHC	4360	2180	2180	0
V_{8-}	$400-500$	TEV	8.14	5.48	2.66	0.35
V_{8-}	$400-500$	LHC	285	145	140	0.017
V_{8+}	$425-525$	TEV	5.93	4.21	1.72	0.42
V_{8+}	$425-525$	LHC	255	130	125	0.021

Table 3. Angular dependences of $t\bar{t}$ production in the η_T and V_8 resonance models with parameters described in the text. Top quarks are produced with pseudorapidity $|\eta| < 2.0$ and cross sections (in pb) have been multiplied by 1.62.

Figure Captions

[1] The $t\bar{t}$ invariant mass distributions, in $p\overline{p}$ collisions at $\sqrt{s} = 1800\,\mathrm{GeV}$, for $m_t = 100 - 220\,\mathrm{GeV}$ in $20\,\mathrm{GeV}$ increments. EHLQ1 distribution functions were used and the cross sections were multiplied by 1.62 as explained in the text. No rapidity cut is applied.

[2] The mean (solid) and root–mean–square (dashed) $t\bar{t}$ invariant mass, as a function of m_t, for $p\overline{p} \to t\bar{t}$ at $\sqrt{s} = 1800\,\mathrm{GeV}$. Lowest–order QCD cross sections (Fig. 1) were used.

[3] The $t\bar{t}$ invariant mass distribution in the presence of a V_8, in $p\overline{p}$ collisions at $\sqrt{s} = 1800\,\mathrm{GeV}$, for $m_t = 175\,\mathrm{GeV}$ and $M_{V_8} = 450\,\mathrm{GeV}$, $\xi_t = \xi_b = -1/\xi_q = \sqrt{40/3}$. The QCD (dotted curve) and the total (solid) rates have been multiplied by 1.62 as explained in the text. No rapidity cut is applied to the top quarks.

[4] The $t\bar{t}$ invariant mass distribution in the presence of a V_8, in $p\overline{p}$ collisions at $\sqrt{s} = 1800\,\mathrm{GeV}$. The parameters and curves are as in Fig. 3 except that $\xi_t = \xi_b = 1/\xi_q = \sqrt{40/3}$.

[5] The $t\bar{t}$ invariant mass distribution in the presence of a V_8, in $p\overline{p}$ collisions at $\sqrt{s} = 1800\,\mathrm{GeV}$, for $m_t = 175\,\mathrm{GeV}$ and $M_{V_8} = 475\,\mathrm{GeV}$, $\xi_t = \xi_b = -1/\xi_q = \sqrt{40/3}$. The curves are labeled as in Fig. 3.

[6] The $t\bar{t}$ invariant mass distribution in the presence of a V_8, in $p\overline{p}$ collisions at $\sqrt{s} = 1800\,\mathrm{GeV}$. The parameters and curves are as in Fig. 5 except that $\xi_t = \xi_b = 1/\xi_q = \sqrt{40/3}$.

[7] The $t\bar{t}$ invariant mass distribution in the presence of an η_T, in $p\overline{p}$ collisions at $\sqrt{s} = 1800\,\mathrm{GeV}$, for $m_t = 175\,\mathrm{GeV}$ and $M_{\eta_T} = 450\,\mathrm{GeV}$, $F_Q = 30\,\mathrm{GeV}$ and $C_t = -1/3$. The QCD (dotted curve), $\eta_T \to t\bar{t}$ and its interference with the QCD amplitude (dashed), and total (solid) rates have been multiplied by 1.62 as explained in the text. No rapidity cut is applied to the top quarks.

[8] The $t\bar{t}$ invariant mass distribution in the presence of an η_T, in $p\overline{p}$ collisions at $\sqrt{s} = 1800\,\mathrm{GeV}$. The parameters and curves are as in Fiig. 7 except that $M_{\eta_T} = 475\,\mathrm{GeV}$.

[9] The effective $t\bar{t}$ mass distribution for $p\overline{p} \to t\bar{t}$ (dotted) and $t_s\bar{t}_s$ (dashed) at $\sqrt{s} = 1800\,\mathrm{GeV}$; $m_{t_s} = 160\,\mathrm{GeV}$ and $m_t = 175\,\mathrm{GeV}$. The solid corve is the sum of the two mass distributions.

[10] The effective $t\bar{t}$ mass distribution for $p\overline{p} \to t\bar{t}$ and $t_s\bar{t}_s$ at $\sqrt{s} = 1800\,\mathrm{GeV}$; $m_{t_s} = 165\,\mathrm{GeV}$ and $m_t = 190\,\mathrm{GeV}$. Curves are labeled as in Fig. 9.

[11] The $\cos\theta^*$ distribution for $p\overline{p} \to t\overline{t}$ at $\sqrt{s} = 1800\,\text{GeV}$ in the presence of a 450 GeV η_T with parameters as in Fig. 7; $430 < \mathcal{M}_{t\overline{t}} < 470\,\text{GeV}$. The components are standard QCD $gg \to t\overline{t}$ (dot-dash), $q\overline{q} \to t\overline{t}$ (long dashes), total QCD (dots), $gg \to \eta_T \to t\overline{t}$ and interference with QCD (short dashes), and the total $d\sigma/\cos\theta^*$ (solid). EHLQ1 distribution functions were used and all cross sections were multiplied by 1.62. The top quarks are required to have pseudorapidity $|\eta| < 2.0$.

[12] The $\cos\theta^*$ distribution for $pp \to t\overline{t}$ at $\sqrt{s} = 15\,\text{TeV}$ in the presence of a 450 GeV η_T with parameters as in Fig. 11; $430 < \mathcal{M}_{t\overline{t}} < 470\,\text{GeV}$. The curves are labeled as in Fig. 11.

[13] The $\cos\theta^*$ distribution for $p\overline{p} \to t\overline{t}$ at $\sqrt{s} = 1800\,\text{GeV}$ in the presence of a 475 GeV V_8 with parameters as in Fig. 5; $400 < \mathcal{M}_{t\overline{t}} < 500\,\text{GeV}$. The components are standard QCD $gg \to t\overline{t}$ (dot-dash), $q\overline{q} \to t\overline{t}$ (long dashes), total QCD (dots), $q\overline{q} \to V_8 \to t\overline{t}$ and interference with QCD (short dashes), and the total $d\sigma/\cos\theta^*$ (solid). EHLQ1 distribution functions were used and all cross sections were multiplied by 1.62. The top quarks are required to have pseudorapidity $|\eta| < 2.0$.

[14] The $\cos\theta^*$ distribution for $pp \to t\overline{t}$ at $\sqrt{s} = 15\,\text{TeV}$ in the presence of a 475 GeV V_8 with parameters as in Fig. 13; $400 < \mathcal{M}_{t\overline{t}} < 500\,\text{GeV}$. The curves labeled as in Fig. 13.

This figure "fig1-1.png" is available in "png" format from:

http://arXiv.org/ps/hep-ph/9501260v1

This figure "fig2-1.png" is available in "png" format from:

http://arXiv.org/ps/hep-ph/9501260v1

This figure "fig3-1.png" is available in "png" format from:

http://arXiv.org/ps/hep-ph/9501260v1

This figure "fig1-2.png" is available in "png" format from:

http://arXiv.org/ps/hep-ph/9501260v1

This figure "fig2-2.png" is available in "png" format from:

http://arXiv.org/ps/hep-ph/9501260v1

This figure "fig3-2.png" is available in "png" format from:

http://arXiv.org/ps/hep-ph/9501260v1

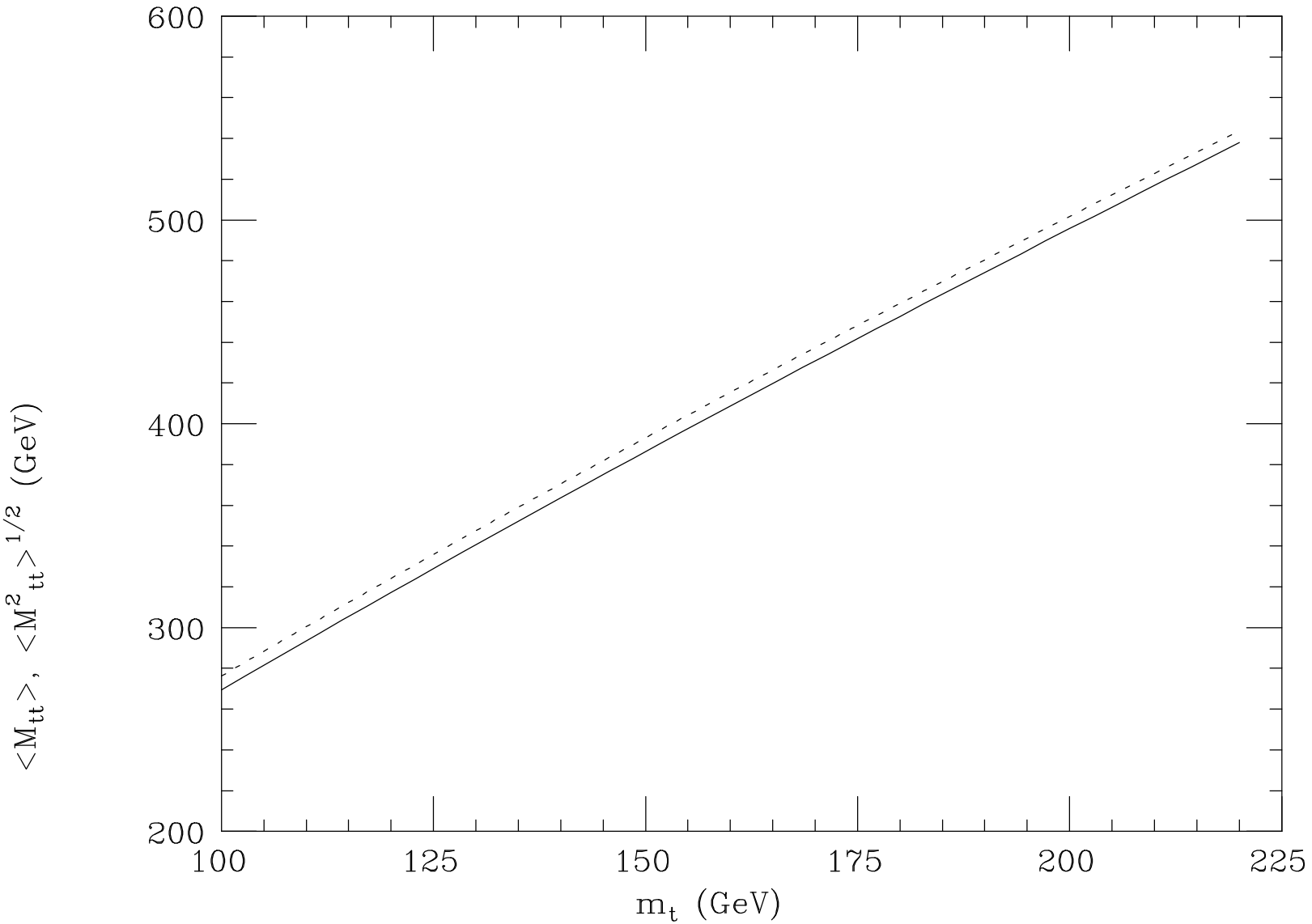
600
500
400
300
200
100
125
150
175
200
225
m_t (GeV)
$<M_{tt}>$, $<M^2_{tt}>^{1/2}$ (GeV)

This figure "fig1-3.png" is available in "png" format from:

http://arXiv.org/ps/hep-ph/9501260v1

This figure "fig2-3.png" is available in "png" format from:

http://arXiv.org/ps/hep-ph/9501260v1

This figure "fig3-3.png" is available in "png" format from:

http://arXiv.org/ps/hep-ph/9501260v1

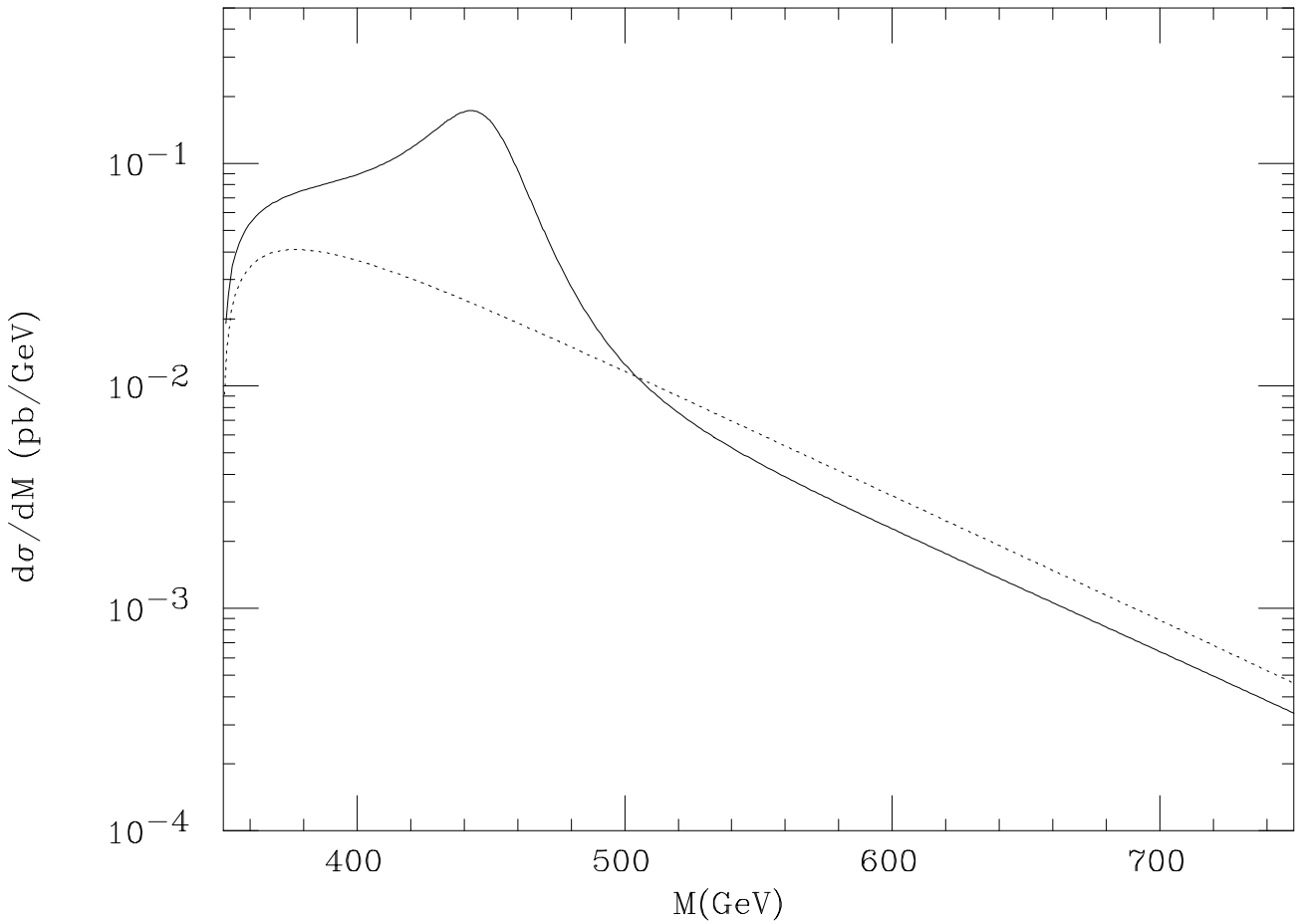
10^{-1}
10^{-2}
10^{-3}
10^{-4}
dσ/dM (pb/GeV)
400
500
600
700
M(GeV)

This figure "fig1-4.png" is available in "png" format from:

http://arXiv.org/ps/hep-ph/9501260v1

This figure "fig2-4.png" is available in "png" format from:

http://arXiv.org/ps/hep-ph/9501260v1

This figure "fig3-4.png" is available in "png" format from:

http://arXiv.org/ps/hep-ph/9501260v1

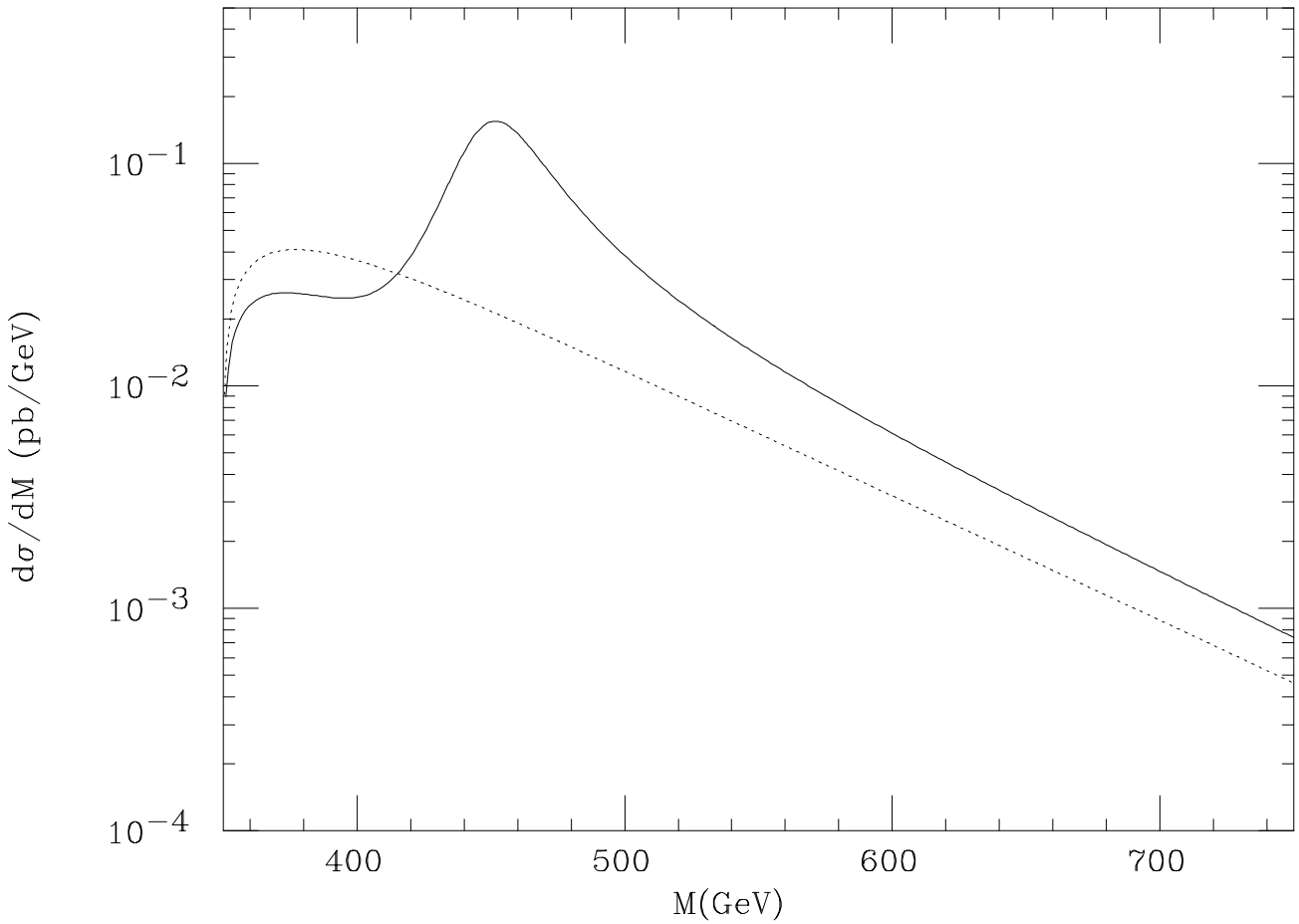
10^{-1}
10^{-2}
10^{-3}
10^{-4}
dσ/dM (pb/GeV)
400
500
600
700
M(GeV)

This figure "fig1-5.png" is available in "png" format from:

http://arXiv.org/ps/hep-ph/9501260v1

This figure "fig2-5.png" is available in "png" format from:

http://arXiv.org/ps/hep-ph/9501260v1

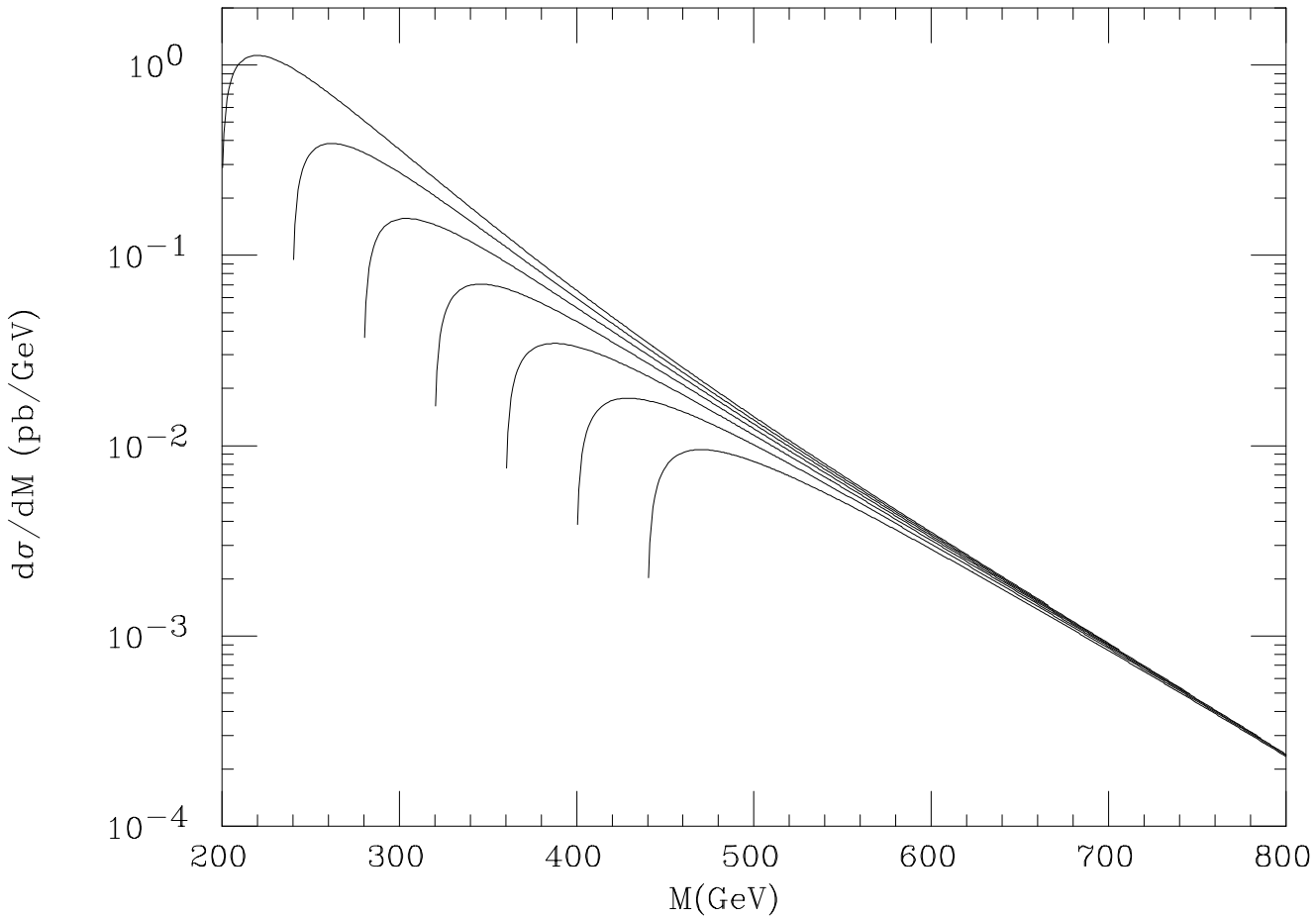
10^0
10^{-1}
10^{-2}
10^{-3}
10^{-4}
dσ/dM (pb/GeV)
200
300
400
500
600
700
800
M(GeV)

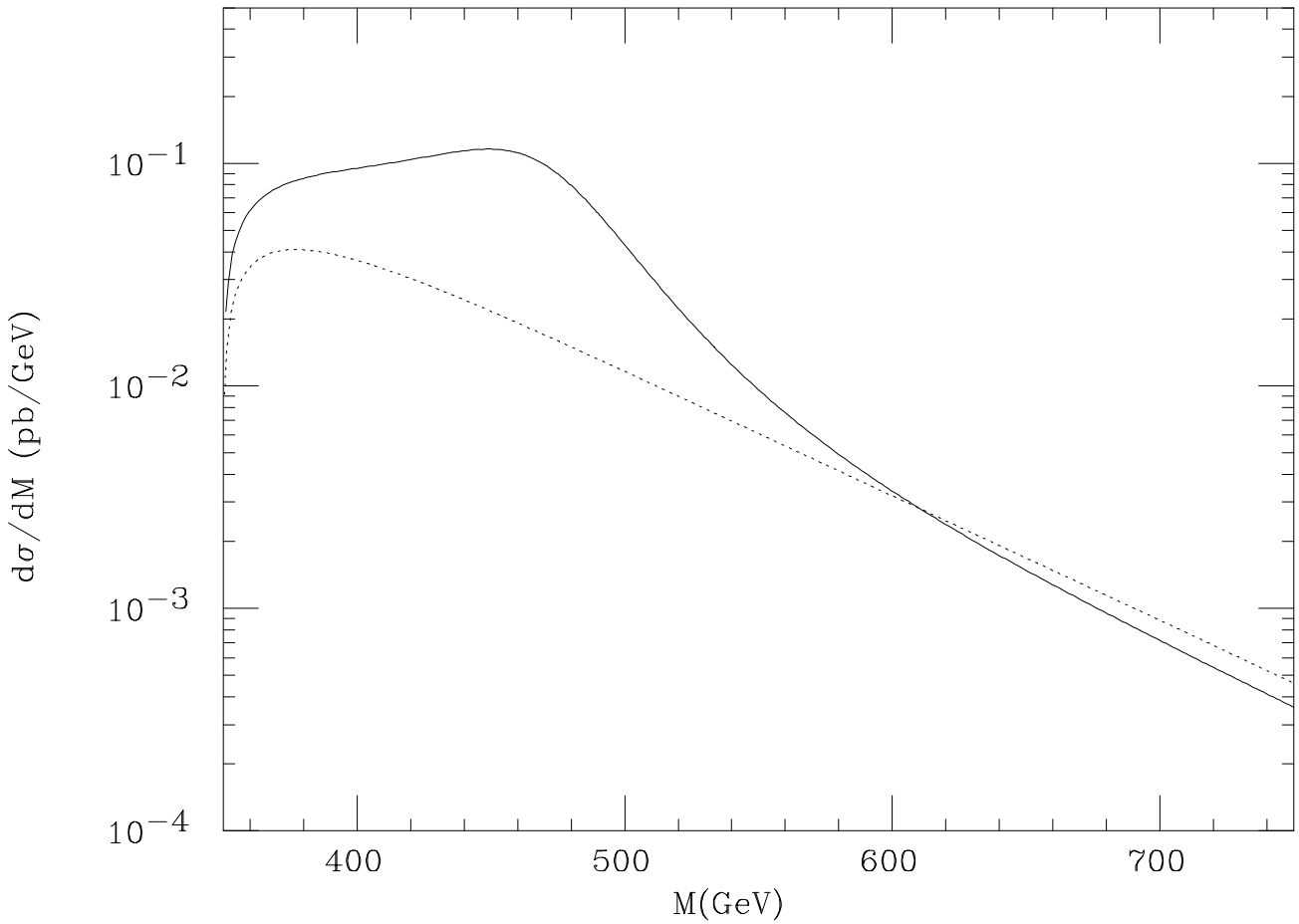
10^{-1}
10^{-2}
10^{-3}
10^{-4}
dσ/dM (pb/GeV)
400
500
600
700
M(GeV)

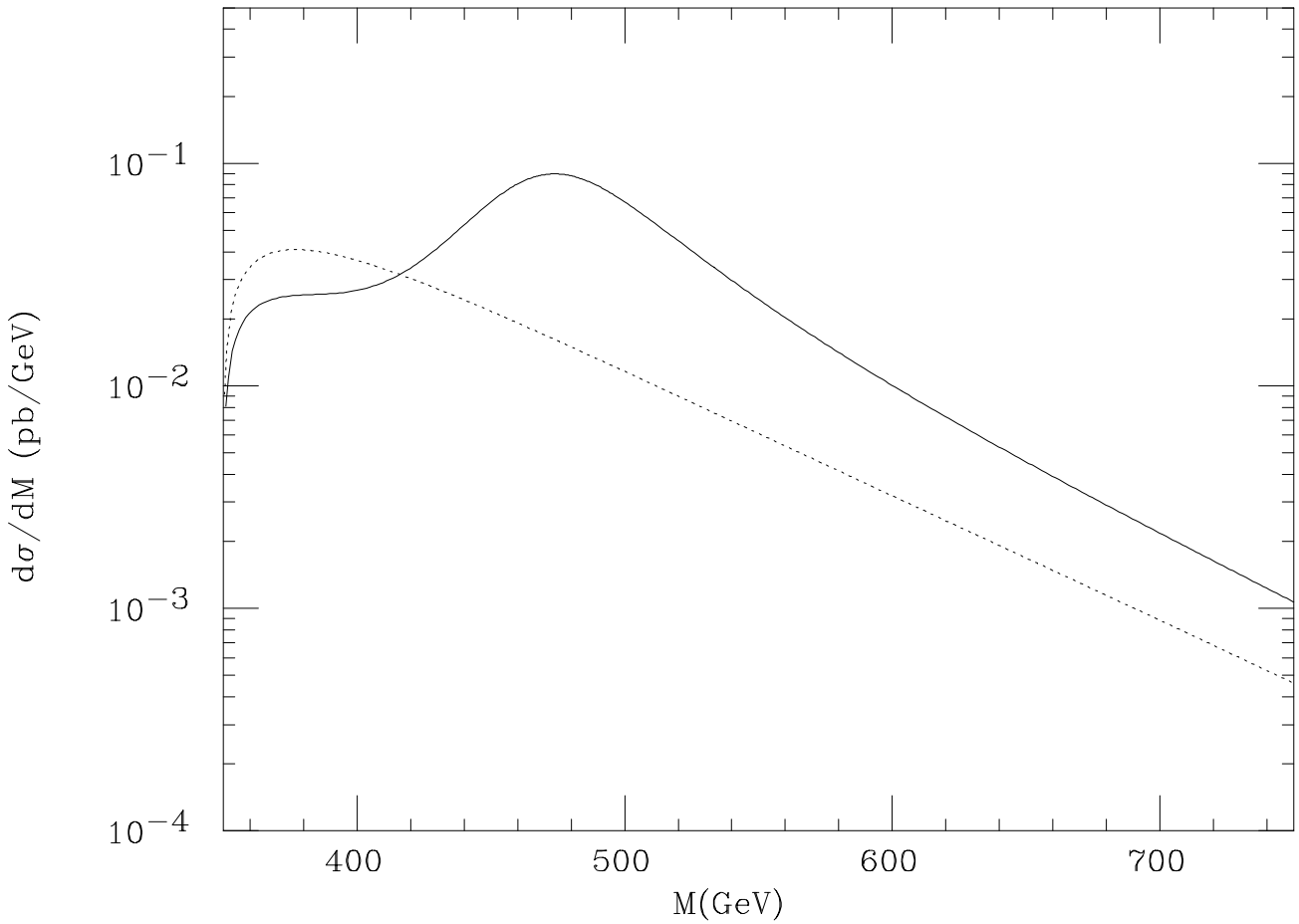
10^{-1}
10^{-2}
10^{-3}
10^{-4}
dσ/dM (pb/GeV)
400
500
600
700
M(GeV)

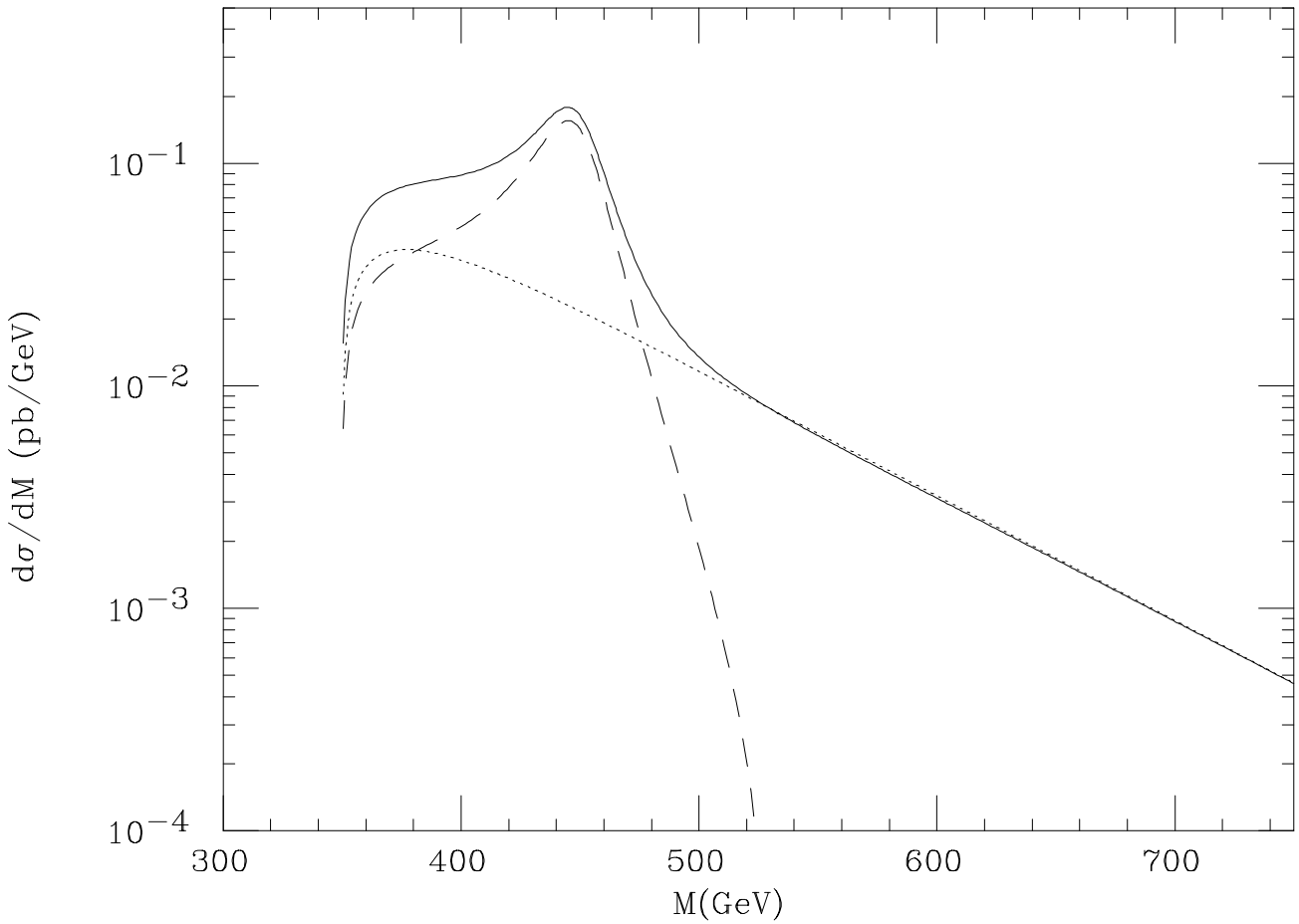
10^{-1}
10^{-2}
10^{-3}
10^{-4}
dσ/dM (pb/GeV)
300
400
500
600
700
M(GeV)

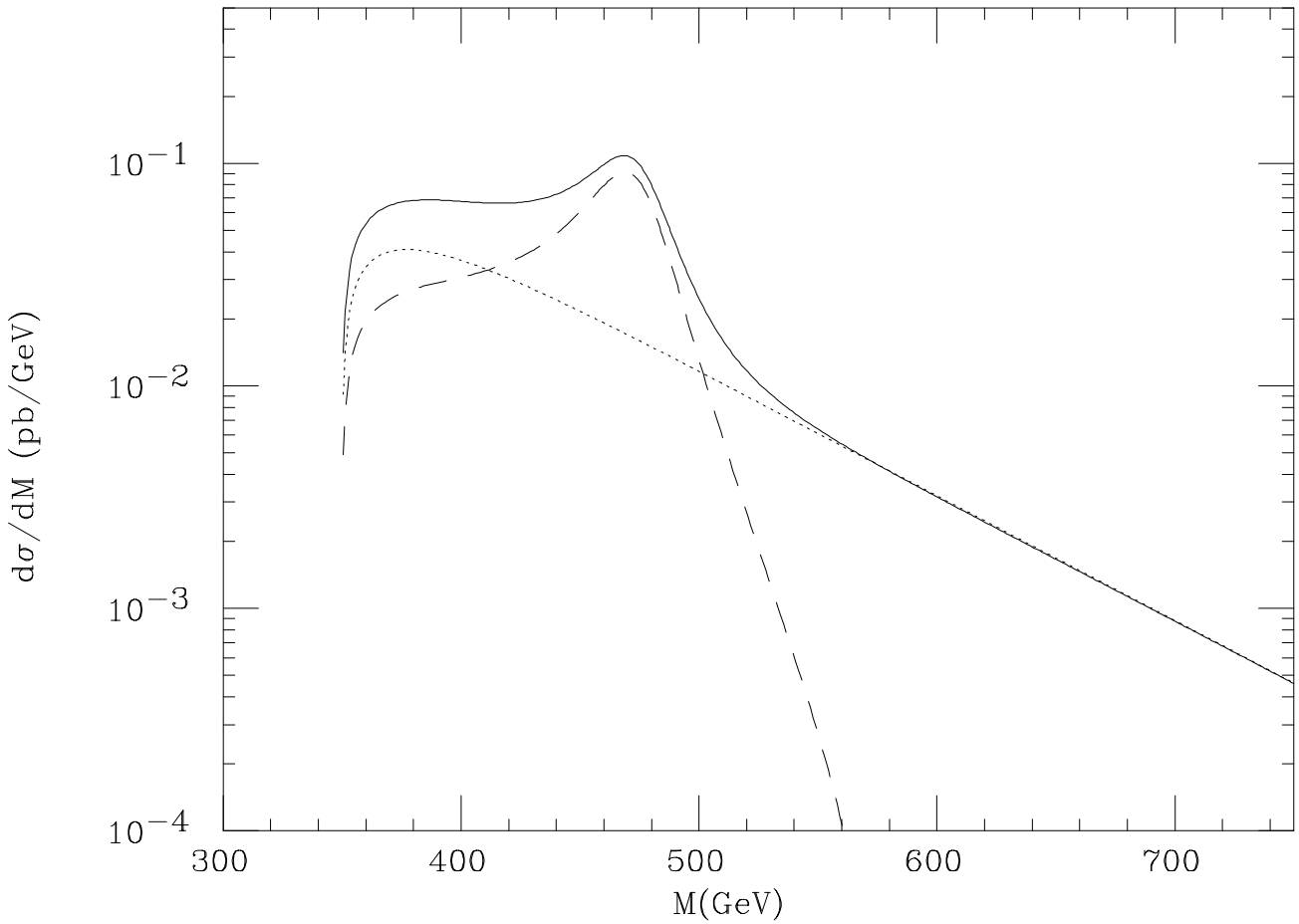
10^{-1}
10^{-2}
10^{-3}
10^{-4}
dσ/dM (pb/GeV)
300
400
500
600
700
M(GeV)

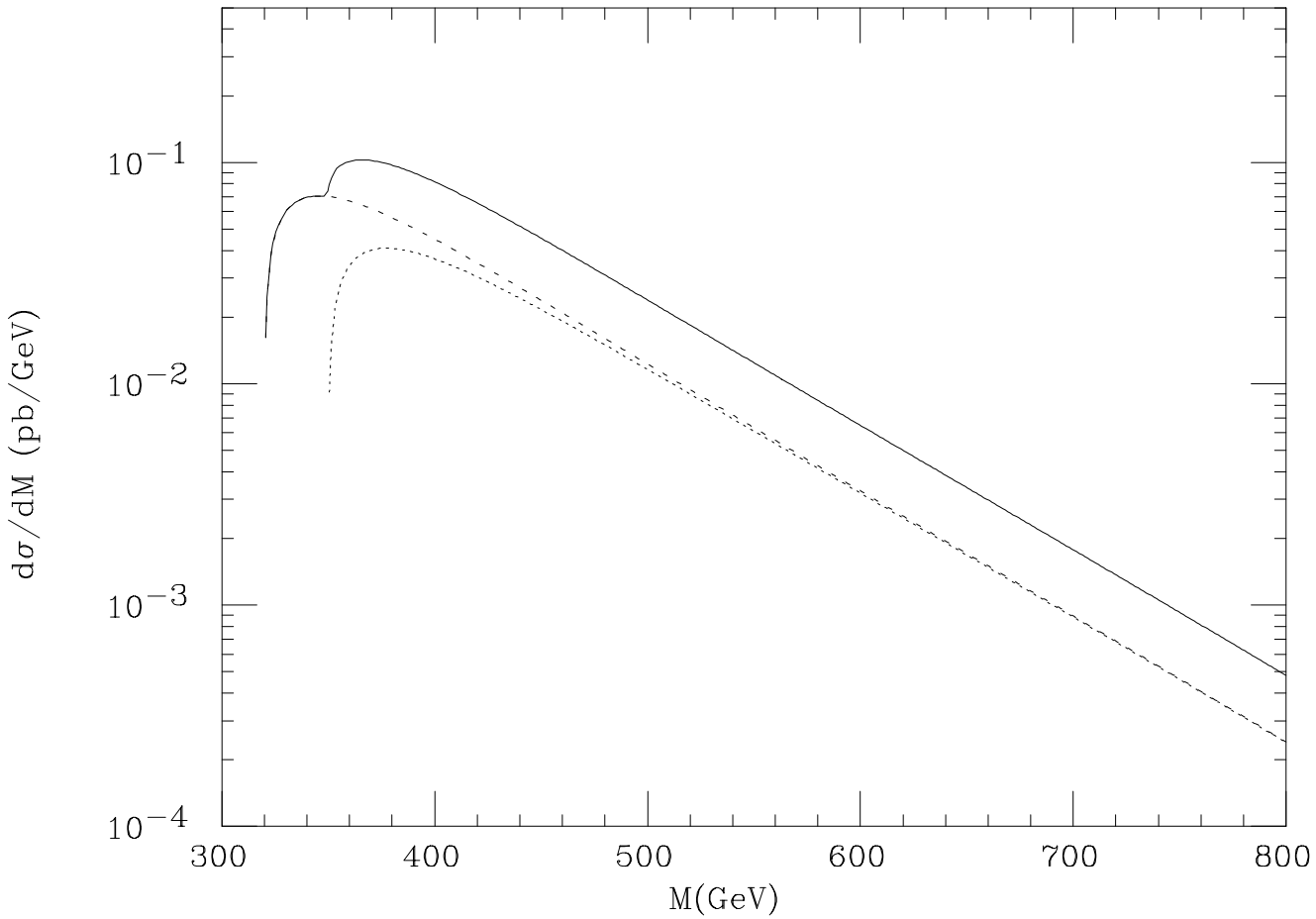
10^{-1}
10^{-2}
10^{-3}
10^{-4}
dσ/dM (pb/GeV)
300
400
500
600
700
800
M(GeV)

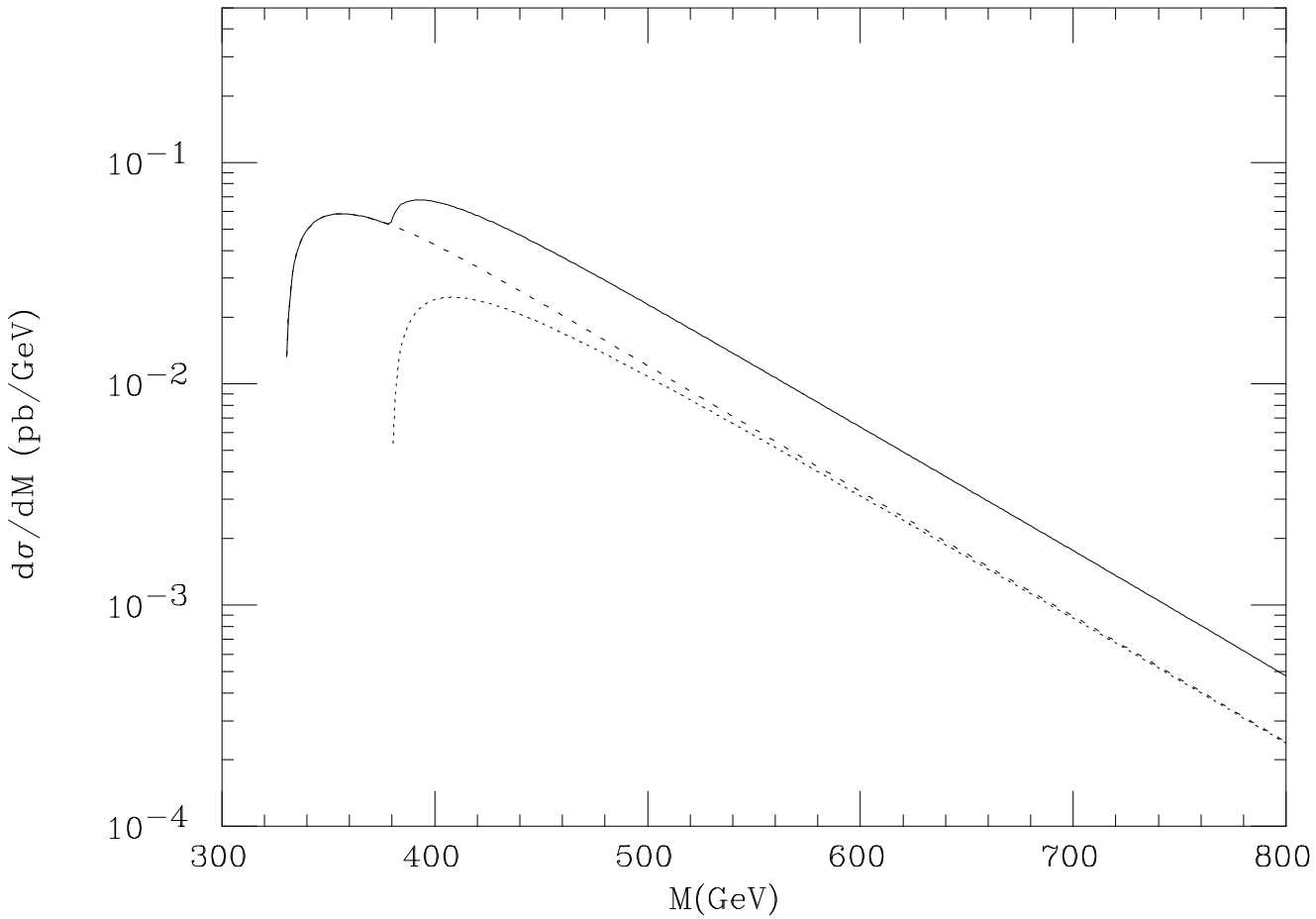
10^{-1}
10^{-2}
10^{-3}
10^{-4}
dσ/dM (pb/GeV)
300
400
500
600
700
800
M(GeV)

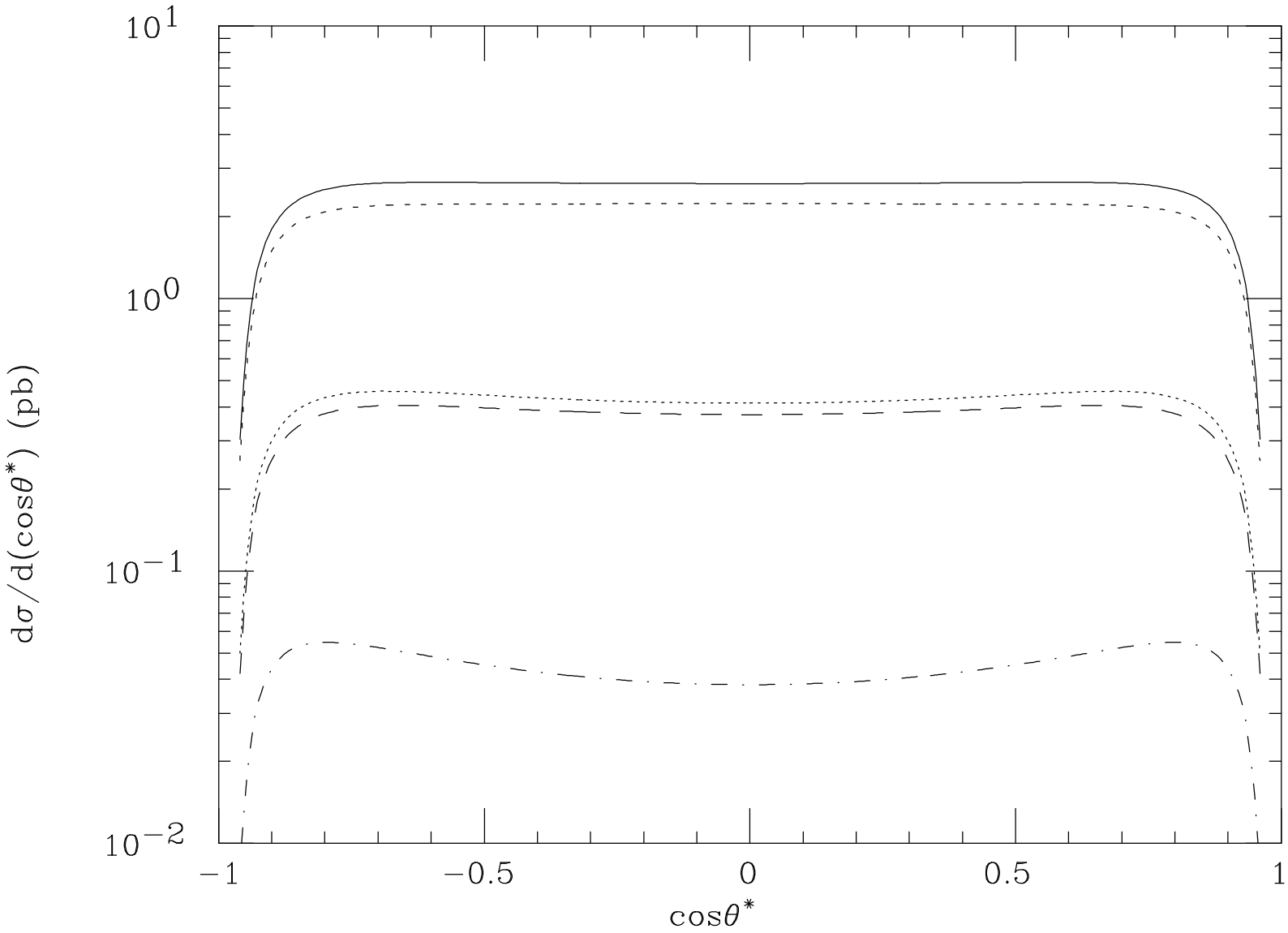
10^1
10^0
10^{-1}
10^{-2}
$d\sigma/d(\cos\theta^*)$ (pb)
−1
−0.5
0
0.5
1
$\cos\theta^*$

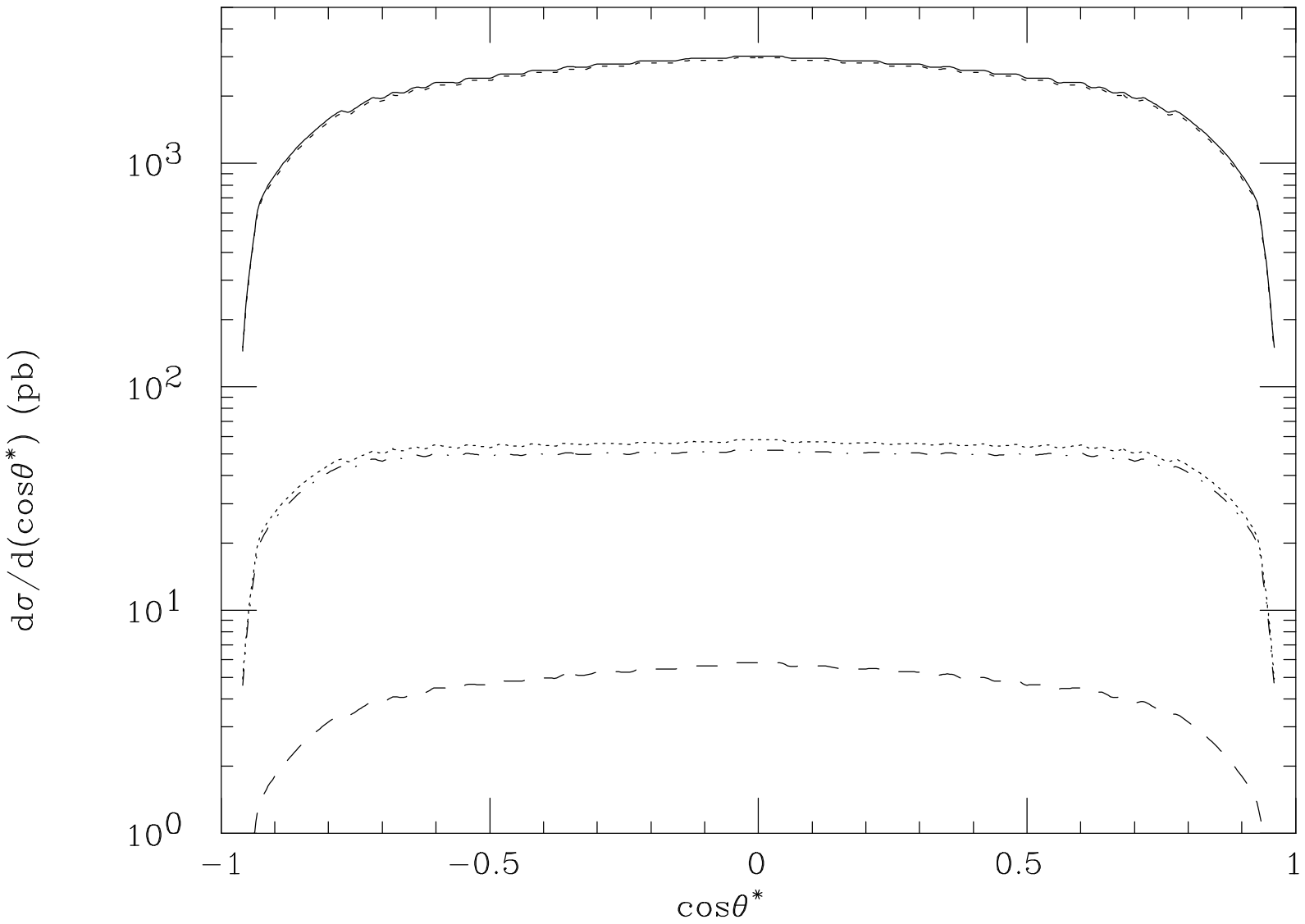
10^3
10^2
10^1
10^0
$d\sigma/d(\cos\theta^*)$ (pb)
−1
−0.5
0
0.5
1
$\cos\theta^*$

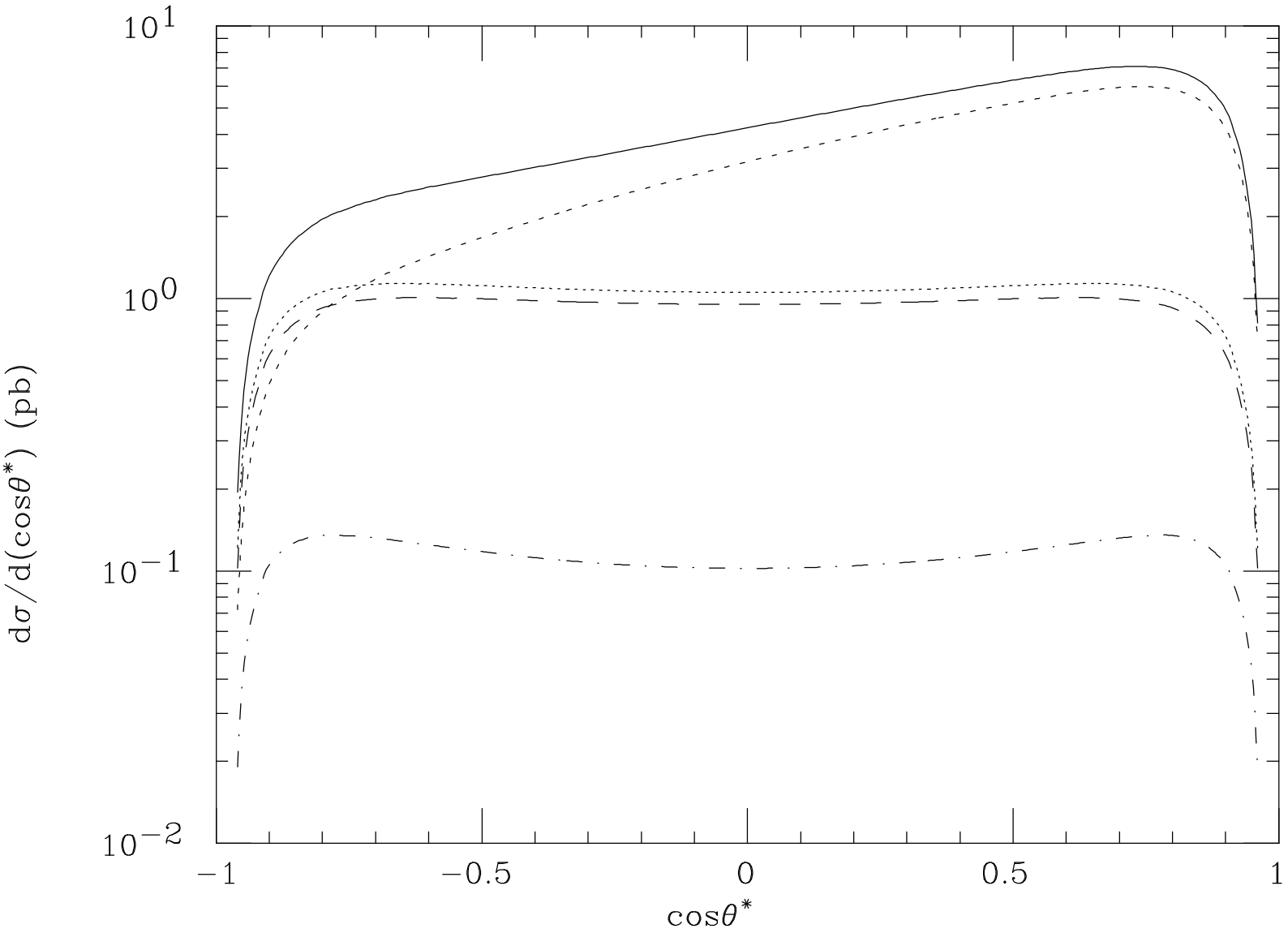
10^1
10^0
10^{-1}
10^{-2}
$d\sigma/d(\cos\theta^*)$ (pb)
−1
−0.5
0
0.5
1
$\cos\theta^*$

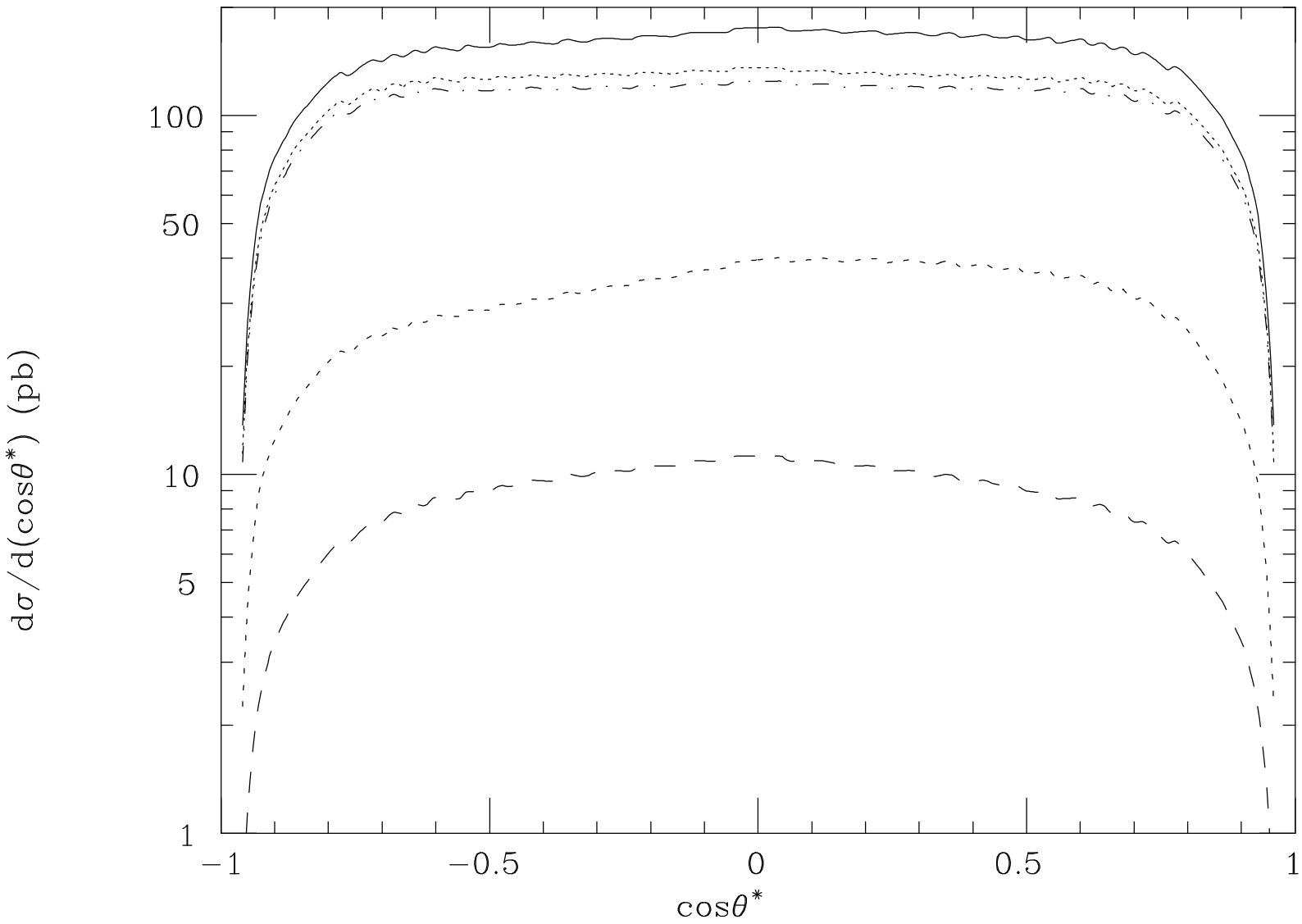
100
50
10
5
1
−1
−0.5
0
0.5
1
dσ/d(cosθ*) (pb)
cosθ*